



HAL
open science

Insights into the Failure Mechanisms of Organic Photodetectors

Marcin Kielar, Mehdi Daanoune, Olivier François-Martin, Bruno Flament, Olivier Dhez, Ajay K Pandey, Sylvain Chambon, Raphaël Clerc, Lionel Hirsch

► **To cite this version:**

Marcin Kielar, Mehdi Daanoune, Olivier François-Martin, Bruno Flament, Olivier Dhez, et al.. Insights into the Failure Mechanisms of Organic Photodetectors. *Advanced Electronic Materials*, 2019, 10.1002/aelm.201700526 . hal-01684953

HAL Id: hal-01684953

<https://hal.science/hal-01684953>

Submitted on 23 Jan 2018

HAL is a multi-disciplinary open access archive for the deposit and dissemination of scientific research documents, whether they are published or not. The documents may come from teaching and research institutions in France or abroad, or from public or private research centers.

L'archive ouverte pluridisciplinaire **HAL**, est destinée au dépôt et à la diffusion de documents scientifiques de niveau recherche, publiés ou non, émanant des établissements d'enseignement et de recherche français ou étrangers, des laboratoires publics ou privés.

Insights into the failure mechanisms of organic photodetectors

Marcin Kielar^{a,d}, Mehdi Daanoun^b, Olivier François-Martin^a, Bruno Flament^a, Olivier Dhez^c,
Ajay K. Pandey^e, Sylvain Chambon^a, Raphaël Clerc^{*b} and Lionel Hirsch^{*a}

- a) Univ. Bordeaux, IMS, CNRS, UMR 5218, Bordeaux INP, ENSCBP, F-33405 Talence, France
- b) Institut d'Optique Graduate School. Université de Lyon, UJM-Saint-Etienne CNRS UMR 5516, Laboratoire Hubert Curien, 42023 Saint-Etienne, France
- c) ISORG, 60 Rue des berges, Parc Polytec, Immeuble Tramontane, 38000 Grenoble, France
- d) Queensland Brain Institute, The University of Queensland, St Lucia, QLD 4072, Australia
- e) School of Electrical Engineering and Computer Science, Queensland University of Technology, Brisbane, QLD 4001, Australia

* Email: raphael.clerc@institutoptique.fr and lionel.hirsch@ims-bordeaux.fr

Abstract

This work investigates in details the reliability of the PCDTBT:PC₆₀BM-based organic photodiodes (OPDs) under visible light and air exposure. The current-voltage (I-V) characteristics of the state-of-the-art OPDs are measured both at room and low temperature, before, during and after ageing. While electrodes are only slightly impacted by ageing, the active layer is significantly damaged regardless the absence of UV light, leading to a major decrease in the responsivity. The combination of the thermally stimulated current (TSC) and the I-V characteristics versus temperature (I-V-T) techniques along with the extensive use of the drift-diffusion simulations all reveal that the observed degradation is the consequence of the generation of shallow traps (0.2 eV, $N_T = 10^{16} \text{ cm}^{-3}$) that significantly reduce the charge carrier mobility. In contrast, deep traps (0.7 eV, $N_T = 7 \times 10^{15} \text{ cm}^{-3}$) are found to be present on freshly prepared samples and their concentration remains unchanged after ageing.

Introduction

Organic electronics is an attractive technology for large area, lightweight and flexible optoelectronic devices.^{[1][2]} Organic photodetectors (OPDs) are among the most promising families of this technology offering several advantages such as broadband spectral selectivity, low cost and low temperature production and solution processability.^[2] These unique properties lead to the development of a range of new products including portable fingerprint sensors, motion or object detectors, human machine interfaces, e-skin or systems for medical imaging.^{[3][4]}

In a recent article,^[5] we demonstrated that organic photodetectors based on poly(2,7-carbazole-alt-4,7-dithienyl-2,1,3-benzothiadiazole) (PCDTBT) and phenyl-C61-butyric acid methyl ester (PC₆₀BM) can reach excellent performances, both in terms of linear dynamic range, external quantum efficiency (EQE > 65% at -2V) and detectivity ($D = 3.2 \times 10^{13} \text{ cm Hz}^{1/2} \text{ W}^{-1}$ at 566 nm and -2 V). These results are essentially the consequence of the low dark current (0.3 nA cm^{-2} at -2 V) achieved thanks to the excellent control of energetic barriers at the electrodes. The energetic barriers were controlled by the introduction of PEIE and PEDOT:PSS organic materials, as reported in the work of Pierre et al.^[6] In the literature, other approaches were also implemented to reduce dark current in organic photodiodes, one can cite the transfer-printing of the P3HT conjugated polymer,^[7] the introduction of p-doped layer by using a soft contact transfer lamination,^[8] the use of a double electron blocking layer,^[9] or the introduction of anionic polyelectrolyte as cathode interlayer.^[10]

It is important to note that the performances of organic photodiodes are comparable with their inorganic counterparts in terms of dark current, responsivity and detectivity. The main

limitation is a relatively low cut-off frequency (\sim hundreds of kHz), being the consequence of the low carrier mobility of organic semiconductors.^[5]

Despite all these recent advances in the field of organic photodiodes, and in contrast to organic solar cells,^[11] the reliability of this technology was not extensively investigated. In addition, since OPDs operate under different conditions, depending on application, it is difficult, if not meaningless, to extrapolate the conclusions valid for solar cells in the field of organic photodiodes. Organic photovoltaic cells in real operating conditions are exposed to both high temperature (> 80 °C) and powerful light intensity (100 mW cm^{-2}) including ultraviolet (UV) radiation. These factors can rapidly become destructive (within a single day) if appropriate encapsulation with suitable materials are not used.^{[12]–[15]} To date, the lifetime of organic solar cells, defined by T_{s80} ,^[16] reached 10,000 hours (~ 417 days),^{[17][18]} and the main limitation is currently attributed to a low power conversion efficiency of the organic cell. In contrast, organic photodiodes are mostly used indoors and are not exposed to UV light, total irradiance power being hundreds, if not thousands, times lower than that used for solar cells. Moreover, their lifetimes are expected to be strongly dependent on their specific operating conditions. Each particular application requires specific spectral range, irradiance level, given light pulse frequency and operating voltage. To date, the OPDs stability over time was investigated in a limited number of publications.^{[3][6][19]} In our previous study,^[5] photodetectors were tested under strong (1 mW cm^{-2}) monochromatic green light. With proper encapsulation, lifetimes over 550 days under continuous illumination were reached. However, an in-depth and systematic characterization is desired in order to achieve a complete understanding of organic photodetector reliability.

The main goal of this work is to further investigate the reliability of organic photodiodes by combining the experiments on the state-of-the-art devices that are validated by robust

numerical simulations. To this aim, the performance of OPDs was monitored in the absence of encapsulation and in the presence of both air and visible light. As expected, lifetimes were drastically reduced and I-V characteristics strongly impacted. In order to understand these failure mechanisms, we present full characterization of OPD devices, before and after ageing, and propose a model to quantitatively describe the nature of defects induced by the combination of air and light.

Experimental section

All details related to sample preparation and device fabrication are described by *Kielar et al.*^[5] Screen-printed poly(3,4-ethylenedioxythiophene):poly(styrenesulfonate) (PEDOT:PSS) was used as organic top electrode for all OPDs, polyethylenimine ethoxylated (PEIE) was used to adjust the indium tin oxide (ITO) bottom electrode work function. The final OPD structure studied in this work was ITO/PEIE/PCDTBT:PC₆₀BM/PEDOT:PSS. The organic materials used in this work along with the complete device structure are presented in Figure 1.

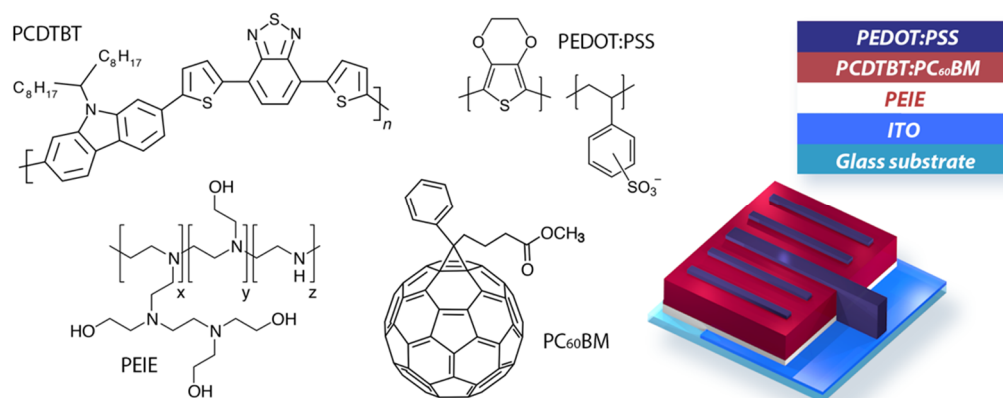


Figure 1: Chemical structures of the organic materials used for OPDs fabrication: PCDTBT (electron donor), PC₆₀BM (electron acceptor), PEIE (ITO-modifier) and PEDOT:PSS (top electrode). The complete device structure is also presented.

For reliability evaluation, a test protocol was developed to continuously measure dark current and photocurrent of the OPD biased at -2V. Photodiodes were under constant green

illumination (528 nm) and light was turned off shortly (3 seconds) to perform a dark current measurement (more details can be found in Figure S1). The OPDs stability was carried out in both air and nitrogen environments (the last one being considered to be a perfect encapsulation). Freshly fabricated and aged samples (8 hours of continuous illumination at 1 mW cm^{-2} in air) were placed under vacuum in the cryostat chamber for TSC and current-voltage characteristics as a function of temperature (I-V-T) studies.

The electrode work function was measured with a *Besocke Delta Phi* Kelvin probe 07 control unit calibrated with highly ordered pyrolytic graphic (HOPG) that was freshly cleaved. Sheet resistance measurements were carried out with *Lucas Labs* four-point probe and with a source measure meter (*Keithley 2400*). UV-Vis absorption spectra were recorded with *SAFAS UVmc2* spectrometer. TSC experiments were carried out using a liquid nitrogen cryostat. A high-power green (528 nm) LED supplied by *Intelligent LED Solutions* was used as light source. An OPD was attached using silver paste to the copper cold-finger of the cryostat and a *Pt100* temperature sensor was placed on the back face of the cold-finger in order to accurately measure the OPD temperature. Current measurements were recorded with a picoammeter (*Keithley 6487*), temperature data with a multimeter (*Keithley 2700*). A custom-built script written in *LabVIEW* environment was developed to record simultaneously both temperature and current as function of time. The linear temperature rise was monitored by a temperature controller. A dual channel source measure unit (*Keithley 2604B*) was used to record the I-V-T. The same cryostat and high-power LED were used for both I-V-T and TSC experiments.

Results and discussion

1/ Evolution of dark current and photocurrent versus time under nitrogen and air

The ageing test has been first carried out for 125 days (1.8×10^5 min) under nitrogen atmosphere. Results are presented in Figure 2a. Both dark and light currents remain almost unchanged during the test period reflecting an excellent stability over time. However, we observed a small decrease in responsivity of the OPD, from 0.30 to 0.27 A W^{-1} .

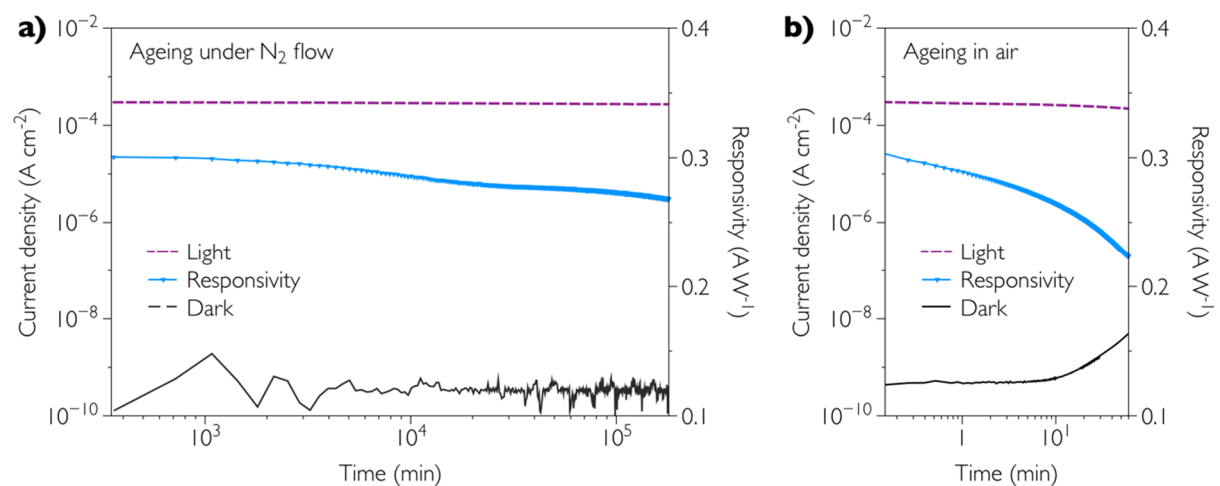


Figure 2: Ageing of an OPD under (a) nitrogen flow and (b) in air. Continuous green illumination of 528 nm was set at 1 mW cm^{-2} . Illumination was switched off during 3s for each dark current point measurement.

The results of the ageing test in air are somehow very different (see Figure 2b) and one can notice a rapid degradation of the responsivity and a fast increase of the dark current. The OPD lifetime is shorter than an hour.

2/ Evidence on the presence of shallow traps by thermally stimulated current technique

Failure mechanisms are usually the consequence of defect and trap formations during ageing. In order to characterize electronic defects in the active layer, TSC and steady state I-V-T were carried out. TSC is a powerful technique to determine the trap density and energy distribution in insulators and semiconductors. Details on the theory of TSC can be found in the seminal papers of Randall et al.,^[20] Haering and Adams,^[21] and Grossweiner.^[22] The goal of this

technique is to fill the traps by an external stimulus that can be either an illumination, a current, a bias, etc. During this stimulation, the sample is frozen at low temperature. Then the stimulus is switched off and the sample is short-circuited. Current is measured while the temperature of the sample is rising. This methodology is summarized in Figure S4, the basic equations are given in Supplementary Information (SI). Simmons et al.^{[23][24]} have extended the theory developed by Haering and Adams,^[25] and proposed to apply a high electric field during the rising of temperature in order to avoid recombination and re-trapping. For OPDs, an internal electric field in the $10^4 - 10^5 \text{ V cm}^{-1}$ range is present at the short circuit conditions due to the difference of electrode work functions. This electric field fits with the requirements of Haering and Adams.^[25]

Freshly prepared and aged (8 hours in air) OPDs were characterized using the TSC technique (Figure 3). Results obtained from TSC are used for modeling that is described in the following section. This is desired in order to reduce the number of free parameters for the simulation.

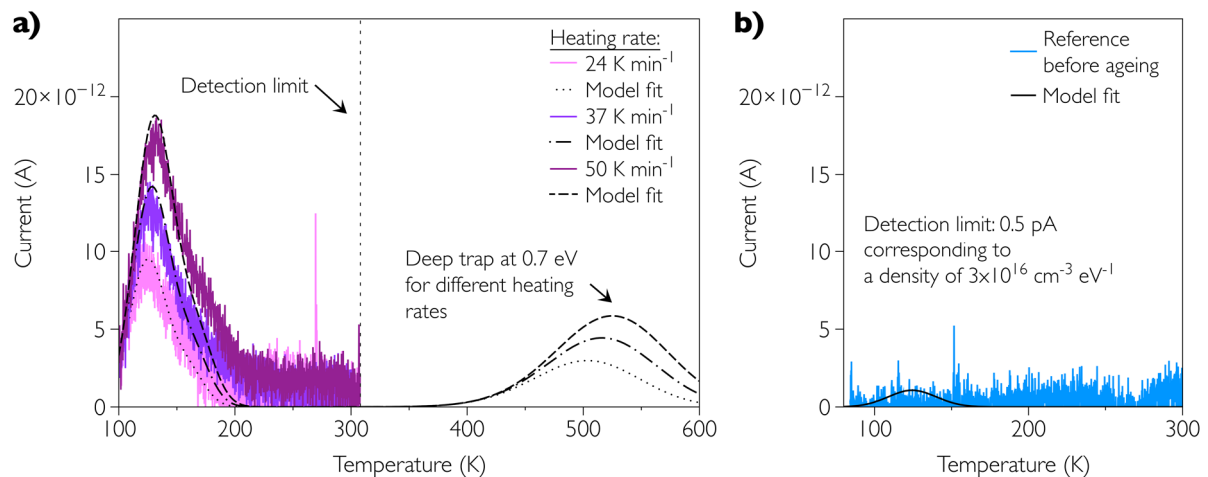


Figure 3: a) Experimental and theoretical Thermally stimulated current (TSC) experiments for different heating rates (24 , 37 and 50 K min^{-1}) for sample aged in air under 1 mW cm^{-2} at 528 nm . b) experimental TSC recorded on a freshly prepared sample, compared with the minimum detectable theoretical signal corresponding to $3 \times 10^{16} \text{ cm}^{-3} \text{ eV}^{-1}$ (equivalent to a total trap concentration of $1.3 \times 10^{15} \text{ cm}^{-3}$).

It is worth emphasizing here that OPDs had to be stressed in air for 8 hours because a rapid OPD degradation observed in Figure 2-b is partially healed once the OPD has been placed

under vacuum in the cryostat. As demonstrated, no traps were detected by the TSC technique on freshly prepared samples, as shown in Figure 3b. Note that the detection limit of our experimental setup is about 0.5 pA. This current corresponds to a minimum detectable trap concentration of $3 \times 10^{16} \text{ cm}^{-3} \text{ eV}^{-1}$ (equivalent to a total trap concentration of $1.3 \times 10^{15} \text{ cm}^{-3}$). Finally, the range of temperature investigated (80-300 K) only allows to probe a limited trap energy range, up to 0.4 eV from the band edge as higher temperature would induce device degradation due to morphological changes in the photoactive layer. In particular, traps located around the middle of the gap, known to induce significant electrons and holes recombination, cannot be detected by the TSC experiments, as shown in Figure 3a.

Table 1: Trap parameters calculated from the experimental TSC study.

	Figure 3a			Figure 3b
	1 st shallow trap	2 nd shallow trap	Deep trap	Detection limit
E_T (eV)	0.16	0.2	0.7	0.16
W_g (eV)	0.05	0.04	0.04	0.05
N_T ($\text{cm}^{-3} \text{ eV}^{-1}$)	2.6×10^{17}	8×10^{16}	9×10^{16}	3×10^{16}
N_T (cm^{-3})	1.13×10^{16}	2.8×10^{15}	3.2×10^{15}	1.3×10^{15}

Regarding aged samples, shallow traps located at 0.16 - 0.2 eV were detected, with a concentration of 10^{16} cm^{-3} . In principle, TSC experiments do not allow to determine if these traps are located close to the HOMO or LUMO band edge of the acceptor/donor active blend. However, our measurements are consistent with the previous reports on the impact of oxygen on organic materials,^{[26]–[28]} known to induce an acceptor trap close to the LUMO level. In the next section, these traps are thus introduced in the simulation as acceptor traps located at 0.16 - 0.2 eV below the LUMO band edge. Only a single level trap was considered for simplicity, even if the TSC experiments have revealed a slightly more complex double Gaussian trap profile (see Table 1).

3/ Modeling approach

Experimental fresh and aged I-V curves as function of temperature were compared with simulations in order to identify the possible ageing mechanism for organic photodiodes. To this aim, 1D drift-diffusion coupled with Maxwell equations were performed using the Fluxim software.^[25] The model particularly includes temperature and field dependent mobility models and donor or acceptor traps within the gap. Following the reference^[29], due to the limited amount of photo-generated charges in organic solar cell and photodiode, the mobility dependency versus photo-generated charges has been neglected. Importantly, the classical Schottky boundary conditions were used,^[30] which consists in keeping the electron and hole concentrations at electrode contacts constant under field and lighting, and equal to their equilibrium values. These concentrations depend on the temperature and on the value of the contact work functions.

To model illuminated current, the optical indexes of the blend were extracted from reflectance and transmittance experiments,^[31] and were used in the simulation. As explained in the experimental section, the source is a green LED with a Gaussian spectrum at 530 ± 5 nm, leading to the irradiance of 0.7 mW cm^{-2} .

The model has several variable parameters, namely: the contact work functions, the parameters of the mobility model and the traps characteristics. In the following part, the procedure used to identify all these parameters on fresh and aged OPD is discussed.

4/ Simulation of the I-V characteristics of virgin devices.

I-V-T plots are presented in Figure 4 for an OPD under illumination before and after 8 hours of ageing in air. Freshly prepared samples are considered at first. The Arrhenius plot of Figure 5, performed on I-V curves biased in direct allows extracting an activation energy of

approximately 0.1 eV. There are two potential origins of this activation energy: activation of the carrier injection at the contact, and activation of the carrier mobility. Note that deep traps do not contribute to the thermal activation of dark and illuminated I-V curves. This is because in the limited temperature range investigated (150 – 300 K), deep traps have only a slight impact on the temperature dependency of I-V due to their high activation energy. To illustrate this point, (see Figure S6), I-V curves have been simulated with only deep traps (without shallow traps, indeed TSC experiments have not revealed any significant shallow traps in virgin devices) and constant mobility. They clearly indicate that deep traps are not responsible of the temperature dependency of experimental IVT curves.

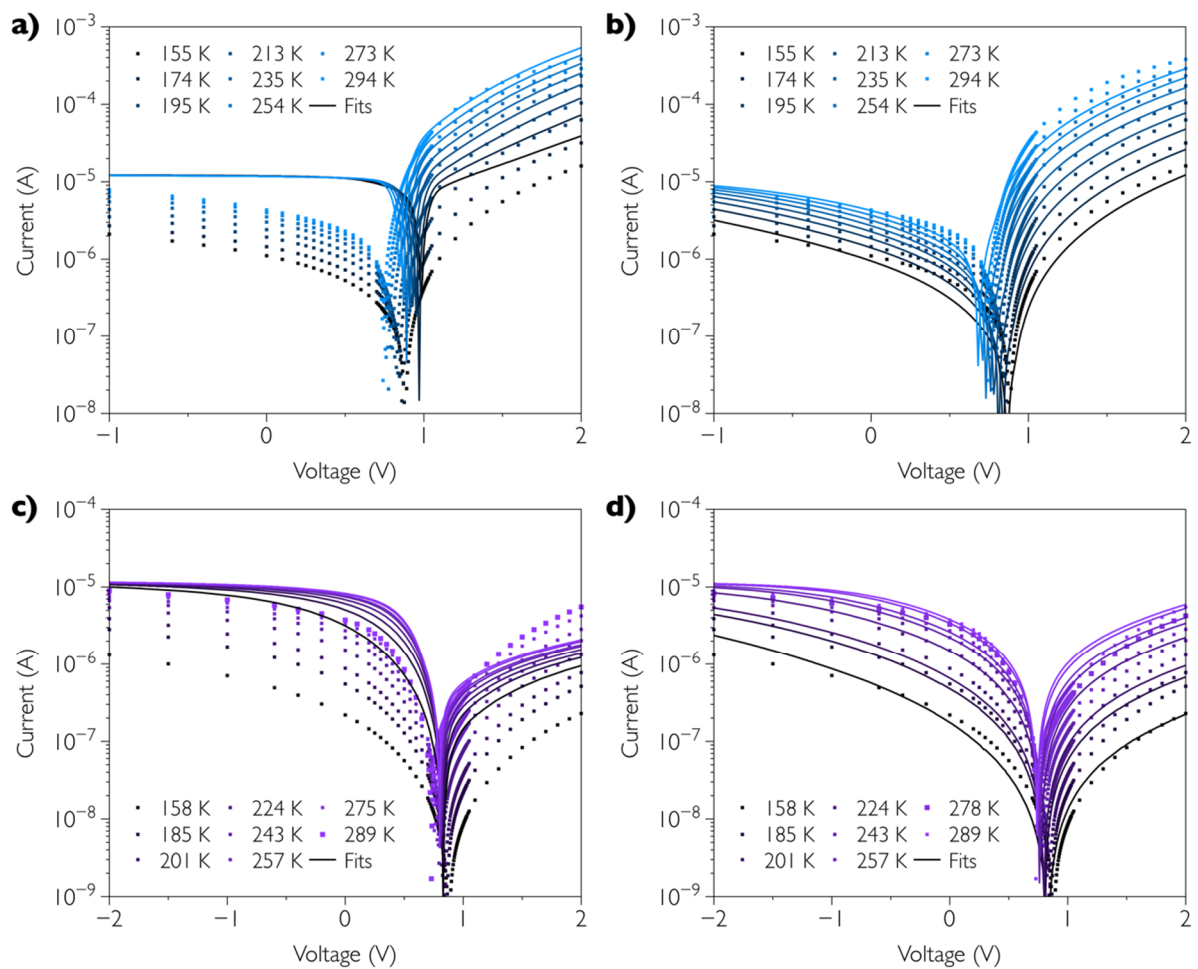


Figure 4: Illuminated I-V curves for virgin and aged devices versus temperature (155 – 290 K), dots are experimental data, solid lines are simulations. a) fresh sample, temperature and field mobility dependent without deep trap were used for simulation. b) fresh sample, temperature, field mobility and deep traps ($E_T=0.7$ eV; $N_T=7 \times 10^{15}$ cm $^{-3}$) were used for simulation. c) aged sample, simulations were performed with, temperature, field mobility, deep traps ($E_T=0.7$ eV; $N_T=7 \times 10^{15}$ cm $^{-3}$) and

without any shallow traps. d) aged sample, simulations include temperature, field mobility both deep ($E_T=0.7$ eV; $N_T=7\times 10^{15}$ cm^{-3}) and shallow traps ($E_{Tshallow}=0.2$ eV; $N_{Tshallow}=1.2\times 10^{16}$ cm^{-3}) according to TSC experiments and mobility degradation.

The work functions of the two electrodes were measured by Kelvin probe in air. We found -5eV for the PEDOT:PSS and -4.17 eV for the ITO/PEIE. These values were used for the numerical simulation (see Table 2).

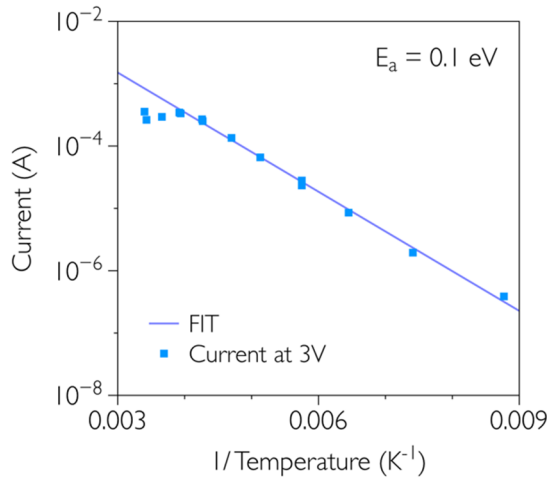


Figure 5: Arrhenius plot performed on virgin dark I-V curves in direct (forward) regime (3V).

A detailed comparison between experimental dark I-V-T curves and simulations have revealed that the mobility was indeed temperature dependent. In particular, as expected from previous works,^{[32][33]} the extracted activation energy was found to be dependent on the applied electric field, which is a signature of mobility dependence with temperature. The ratio of PCDTBT electrons and holes mobilities has been found to be between 0.1 and 10,^[34] depending on process conditions. Moreover, Abbas and Tekin have shown that optimized solar cells have balanced charge carrier mobilities.^[35] For these reasons, both electron and hole mobilities have been assumed equal ($\mu_0 = \mu_n = \mu_p$) in a first-order approximation. Therefore, the following mobility model were used:

$$\mu(E, T) = \mu_0 \exp\left(-\frac{E_\mu}{kT}\right) \exp(\gamma(T)\sqrt{E}) \quad (1)$$

$$\gamma(T) = B \left(\frac{1}{kT} - \frac{1}{kT_0} \right) \quad (2)$$

Where E is the local electric field. An order of magnitude of the B and T_0 parameters can be extracted from the slope of $\ln I$ versus $E^{3/2}$ versus temperature (where I is the direct dark current at high electric field i.e. $V > 1$ V).

The extraction of all parameters was performed by fitting both the dark and illuminated current. All the above-mentioned experiments were used to reduce the number of free parameters. Table 2 summarizes the parameters used in simulation (Figure 4).

Table 2: Parameters used in simulation presented in Figure 5.

Fresh photodiodes		
Work function (eV)	-5 (PEDOT:PSS)	-4.17 (ITO/PEIE)
μ_0 cm ² /V.s	$\mu_n = \mu_p = 0.03$	
B eV. (m/V) ^{0.5}	1.5×10^{-5}	
T ₀ (K)	1000	
E _a (eV)	0.08	
Active layer thickness (nm)	400	
Active area (m ²)	2.5×10^{-6}	
Trap parameters: for a single trap		
E _T (eV)	0.7	
N _T (cm ⁻³)	7×10^{15}	
C _p /C _n (cm ³ /s)	10^{-10}	
Aged photodiodes		
Work function (eV)	-5 (PEDOT:PSS)	-4.27 (ITO/PEIE)
μ_0 cm ² /V.s	$\mu_n = 0.001$ $\mu_p = 3 \times 10^{-4}$	
B eV. (m/V) ^{0.5}	1.5×10^{-5}	
T ₀ (K)	1000	
E _a (eV)	0.08	
Active layer thickness (nm)	400	
Active area (m ²)	2.5×10^{-6}	
Trap parameters	Deep trap	Acceptor like TSC Trap
E _T (eV)	0.7	0.2 (below the LUMO)
N _T (cm ⁻³)	7×10^{15}	10^{16}
C _p /C _n (cm ³ /s)	10^{-10}	10^{-10}

Even if the deep traps do not impact the temperature dependency of both dark and illuminated I-V curves, they clearly impact the global shape of I-V-T curves, and in particular the level of photocurrent. As example, the Figure 4a and Figure 4b present a comparison

between experimental illuminated current and simulations performed with and without deep traps. It clearly indicates the presence of deep traps even though they cannot be characterized by TSC as due to the detection limit (see Figure 3a).

5/ Simulation of the I-V characteristics of aged devices.

Aged samples are presented in Figure 4c and d. In the reverse regime, the illuminated current is lower in the aged device than in the virgin device, leading to a 20 % decrease of sensitivity at 290 K (at -2V). This discrepancy increases at lower temperature. In the forward regime, surprisingly, the difference between virgin and aged I-V curves appears even more significant, but it is essentially the consequence of a strong reduction of the direct dark current.

The fittings of I-V curves were performed by the following procedure. Firstly, work functions were kept approximately constant. Only a moderate ~ 0.1 eV modification of the ITO/PEIE was introduced according to the experimental results obtained by Kelvin probe (see Table S1 in SI). As PEDOT:PSS electrodes did not show any significant modification (see Figure S2 in SI), its work function has been considered as constant. Secondly, the irradiance level was kept identical before and after ageing, the traps by TSC experiments were detected (single energy level at 0.2 eV below the LUMO level with a concentration of 10^{16} cm $^{-3}$), keeping the concentration of deep traps unchanged.

In a first attempt to reproduce experiments (not shown here), mobility was also kept unchanged, and in this latter case, it was not possible to achieve a decent fit of experimental results, (except if the concentration of shallow traps at 0.2 eV was highly increased to the unrealistic level of 10^{19} cm $^{-3}$ instead of 10^{16} cm $^{-3}$ according to TSC experiments). It was also not possible to fit data by only tuning the deep trap concentrations. Therefore, in order to highlight the critical impact of the shallow traps measured by the TSC experiments in the

temperature dependence in the reverse regime the effect of shallow traps we have plotted the modeling with only deep traps in Figure 4c.

Consequently, using the same procedure for fresh devices, the parameters of the mobility model were also adjusted, suggesting that the ageing of devices was also responsible for a degradation of the mobility. The best fits on illuminated I-V curves versus temperature obtained using this approach are shown in Figure 4d. All parameters used in the simulation are reported in Table 2. Even though such degradation of the mobility due to ageing is plausible, it can also be due to either the impact of the negative charges trapped (coulomb centers) or a degradation of the polymer itself, penalizing charge transport.

Conclusion

In this work, the ageing study of the state-of-the-art PCDTBT:PC₆₀BM organic photodiodes under visible light and in air was conducted by the use of three different techniques: thermally stimulated current, I-V experiments versus temperature and drift-diffusion simulations.

From a qualitative point of view, it was shown that appropriate encapsulation protects the devices from the failure mechanisms even after four months of continuous and powerful illumination. The combined presence of light and air induces a rapid degradation of OPDs that can partially be healed once the OPD is placed under vacuum. Electrodes were found stable even after several days of exposure to air and light. On the opposite, the active layer was found significantly damaged, regardless the absence of UV light, causing a decrease of the device responsivity at room temperature.

The drift-diffusion simulations were carried out to quantify the traps induced by the combination of light and air. We have shown that the OPD degradation was the consequence of the generation of shallow traps that can be fully characterize by thermally stimulated

current. That being said, our experiments establish that even though ageing is causing both formation of shallow traps and charge carrier mobility degradation by two orders of magnitude, the OPD responsivity is only 20% reduced at high applied voltage -2V.

Clearly, the nature and extent of degradation to OPDs are very different to OPVs. Finally, deep traps are present in freshly prepared samples and their concentration is not affected by the ageing in air.

Acknowledgements

This work has also been funded by the French National Research Agency (ANR) through the TAPIR project N° ANR-15-CE24-0024-01 and by LabEx AMADEus (ANR-10- LABX-0042- AMADEUS through grant ANR-10-IDEX-0003-02). This work has also been co-funded by the Région Nouvelle Aquitaine through the TAMANOIR project no. 2016-1R10105.

References

- [1] Y.S. Rim, S.-H. Bae, H. Chen, N. De Marco, Y. Yang, *Adv. Mater.* **2016**, *28*, 4415.
- [2] R.D. Jansen-van Vuuren, A. Armin, A.K. Pandey, P.L. Burn, P. Meredith, *Adv. Mater.* **2016**, *28*, 4766.
- [3] T.N. Ng, W.S. Wong, M.L. Chabiny, S. Sambandan, R.A. Street, *Appl. Phys. Lett.* **2008**, *92*, 213303.
- [4] M. Caironi, Y.-Y. Noh, *Large Area and Flexible Electronics*, Wiley-VCH**2015**.
- [5] M. Kielar, O. Dhez, G. Pecastaings, A. Curutchet, L. Hirsch, *Sci. Rep.* **2016**, *6*, 39201.
- [6] A. Pierre, I. Deckman, P.B. Lechêne, A.C. Arias, *Adv. Mater.* **2015**, *27*, 6411.
- [7] S. Xiong, L. Li, F. Qin, L. Mao, B. Luo, Y. Jiang, Z. Li, J. Huang, Y. Zhou, *ACS Appl. Mater. Interfaces* **2017**, *9*, 9176.
- [8] J. Herrbach, A. Revaux, D. Vuillaume, A. Kahn, *Appl. Phys. Lett.* **2016**, *109*, 73301.
- [9] S. Shafian, H. Hwang, K. Kim, *Opt. Express* **2016**, *24*, 25308.
- [10] S. Yoon, J. Cho, K.M. Sim, J. Ha, D.S. Chung, *Appl. Phys. Lett.* **2017**, *110*, 83301.
- [11] P. Cheng, X. Zhan, H.-M. Kim, J.-H. Youn, D.-H. Nam, Y.-G. Lee, J.-G. Lee, A.R.B.M. Yusoff, J. Jang, S. Graham, M. Chhowalla, W.C.H. Choy, F. Li, J. Peng, Y. Cao, S.R.P. Silva, C. Müller, A. Rivaton, G.Y. Uzunoglu, D.S. Germack, M. Hosel, H.F. Dam, M. Jorgensen, S.A. Gevorgyan, M. V. Madsen, E. Bundgaard, F.C. Krebs, K. Norrman, M. Xiao, J. Hauch, R. Steim, D.M. DeLongchamp, R. Rösch, H. Hoppe, N. Espinosa, A. Urbina, G. Yaman-Uzunoglu, J.-B. Bonekamp, A.J.J.M. van Breemen, C. Girotto, E. Voroshazi, F.C. Krebs, *Sol. Energy Mater. Sol. Cells* **2013**, *111*, 97.

- [12] W. Greenbank, L. Hirsch, G. Wantz, S. Chambon, *Appl. Phys. Lett.* **2015**, *107*, 263301.
- [13] K. Norrman, S.A. Gevorgyan, F.C. Krebs, *ACS Appl. Mater. Interfaces* **2009**, *1*, 102.
- [14] *Sol. Energy Mater. Sol. Cells* **2006**, *90*, 213.
- [15] S. Chambon, A. Rivaton, J.-L. Gardette, M. Firon, L. Lutsen, *J. Polym. Sci. Part A Polym. Chem.* **2007**, *45*, 317.
- [16] S.A. Gevorgyan, N. Espinosa, L. Ciammaruchi, B. Roth, F. Livi, S. Tsopanidis, S. Züfle, S. Queirós, A. Gregori, G.A. dos R. Benatto, M. Corazza, M. V. Madsen, M. Hösel, M.J. Beliatis, T.T. Larsen-Olsen, F. Pastorelli, A. Castro, A. Mingorance, V. Lenzi, D. Fluhr, R. Roesch, M. Maria Duarte Ramos, A. Savva, H. Hoppe, L.S.A. Marques, I. Burgués, E. Georgiou, L. Serrano-Luján, F.C. Krebs, *Adv. Energy Mater.* **2016**, *6*, 1600910.
- [17] S.A. Gevorgyan, I.M. Heckler, E. Bundgaard, M. Corazza, M. Hösel, R.R. Søndergaard, G.A. dos Reis Benatto, M. Jørgensen, F.C. Krebs, *J. Phys. D: Appl. Phys.* **2017**, *50*, 103001.
- [18] Y. Zhang, H. Yi, A. Iraqi, J. Kingsley, A. Buckley, T. Wang, D.G. Lidzey, *Sci. Rep.* **2017**, *7*, 1305.
- [19] W. Li, D. Li, G. Dong, L. Duan, J. Sun, D. Zhang, L. Wang, *Laser Photon. Rev.* **2016**, *10*, 473.
- [20] J.T. Randall, M.H.F. Wilkins, *Proc. R. Soc. London A Math. Phys. Eng. Sci.* **1945**, *184*.
- [21] K.H. Nicholas, J. Woods, *Br. J. Appl. Phys.* **1964**, *15*, 783.
- [22] L.I. Grossweiner, *J. Appl. Phys.* **1953**, *24*, 1306.
- [23] J.G. Simmons, M.C. Tam, *Phys. Rev. B* **1973**, *7*, 3706.
- [24] J.G. Simmons, G.W. Taylor, *Phys. Rev. B* **1972**, *5*, 1619.
- [25] E. Knapp, R. Häusermann, H.U. Schwarzenbach, B. Ruhstaller, *J. Appl. Phys.* **2010**, *108*, 54504.
- [26] J. Schafferhans, A. Baumann, A. Wagenpfahl, C. Deibel, V. Dyakonov, **2010**.
- [27] A. Seemann, T. Sauermann, C. Lungenschmied, O. Armbruster, S. Bauer, H.-J. Egelhaaf, J. Hauch, *Sol. Energy* **2011**, *85*, 1238.
- [28] V. Kazukauskas, *Semicond. Sci. Technol.* **2004**, *19*, 1373.
- [29] F. Deledalle, P. Shakya Tuladhar, J. Nelson, J.R. Durrant, T. Kirchartz, *J. Phys. Chem. C* **2014**, *118*, 8837.
- [30] S.M. Sze, K.K. Ng, *Physics of Semiconductor Devices*, Wiley-Interscience **2007**.
- [31] A.B. Djurišić, T. Fritz, K. Leo, *Opt. Commun.* **2000**, *183*, 123.
- [32] H.K.H. Lee, Z. Li, I. Constantinou, F. So, S.W. Tsang, S.K. So, *Adv. Energy Mater.* **2014**, *4*, 1400768.
- [33] K.K.H. Chan, S.W. Tsang, H.K.H. Lee, F. So, S.K. So, *Org. Electron.* **2012**, *13*, 850.
- [34] S. Alem, T.-Y. Chu, S.C. Tse, S. Wakim, J. Lu, R. Movileanu, Y. Tao, F. Bélanger, D. Désilets, S. Beaupré, M. Leclerc, S. Rodman, D. Waller, R. Gaudiana, *Org. Electron.* **2011**, *12*, 1788.
- [35] M. Abbas, N. Tekin, *Appl. Phys. Lett.* **2012**, *101*, 73302.